SAND2020-5017C

A Reactive Molecular Dynamics Study of Phenol and Phenolic Polymers in Extreme Environments

Keith Jones[1,a)], J. Matthew D. Lane[1] and Nathan W. Moore[1]

[1]*Sandia National Laboratories, Albuquerque, NM 87185 USA*

[a)]Corresponding author: keijone@sandia.gov

Abstract. Phenolic polymers are key components in carbon composites used in heat shielding due to their ablative properties, and are oftentimes exposed to extreme conditions such as heating and shock. Our ability to model these systems requires an understanding of shock induced chemical pathways. In this work, three parametrizations of the ReaxFF classical MD potential are compared in their ability to model phenolic polymers under shock induced chemistry. We calculate the activation energies associated with both the formation of water, and the liberation of volatile compounds via an Arrhenius analysis of several constant temperature pyrolysis simulations. The activation energies for all three parametrizations are in agreement with the experimental thermogravimetric analysis (TGA) results. We also study phenol, a relevant model system with a well-defined structure. We compare the density of phenol, for temperatures ranging from 123 K to 423 K. The accuracy of the density of phenol at various temperatures serves as an indicator for the ability of a given parametrization to predict density of a phenolic polymer under shock.

INTRODUCTION

Reactive molecular dynamics (MD) can provide insight into the processes that occur during heating and shock, as well as the relationship between the molecular structure and the density, shock response, and mechanisms of pyrolytic breakdown—a valuable link between microscopic properties and macroscopic observables. For example, depending on the curing conditions, phenolic polymers can vary greatly in crosslink extent, initial density, stoichiometry, and molecular structure [1, 2]. Each of these factors modulates the hydrogen bonding topology, which has been shown with MD to play a role in the thermal-mechanical properties of phenolic polymers [3]. Hydrogen bonding interactions are intermolecular interactions that phenolic polymers exhibit due to the hydroxyl groups throughout the structure.

The shock response of phenolic polymer has been shown to exhibit a shoulder or cusp in its ρ, P Hugoniot near 25 GPa [4]. Arman et al [5] concluded that the cusp is likely due to the onset of chemistry, because non-reactive simulations were unable to reproduce the Hugoniot feature. We seek an accurate high-pressure reactive force field in order to investigate the chemical pathways that occur in this regime. In this work, we investigate the ability of three ReaxFF MD parametrizations to model compression and to model chemistry during pyrolysis that can occur during high pressure shock in phenolics.

ReaxFF is a bond order MD potential that handles chemistry [6], with parametrizations for various combinations of elements and conditions. We chose the ReaxFF parametrizations by Chenoweth et al. [7], Mattsson et al. [8], and a hybrid parametrization that we developed specifically for this work which capitalizes on the properties of the Chenoweth and Mattsson parametrizations. The Chenoweth parametrization excels in hydrocarbon reactivity and oxidation and has been employed to study phenolic pyrolysis [9–14]. However, ambient densities are high with this parametrization. The Mattsson parametrization has been used for hydrocarbon polymers subject to high-rate thermal degradation [15] and under shock induced chemistry, in agreement with experimental results [8, 16]. However, this parametrization is untested for oxygen containing systems. Our hybrid ReaxFF parametrization capitalizes on the shock compression capabilities of the Mattsson parametrization, but utilizes the O-H — O hydrogen bonding parameters of the Chenoweth parametrization. Although the change was minor, this heuristic approach is not a standard way to develop an MD potential, so we tested this hybrid under various conditions in this work to probe its suitability for simulating phenolic polymers under shock induced chemistry.

Using the three ReaxFF parametrizations, we calculated the activation energies associated with the formation of

Sandia National Laboratories is a multimission laboratory managed and operated by National Technology & Engineering Solutions of Sandia, LLC, a wholly owned subsidiary of Honeywell International Inc., for the U.S. Department of Energy's National Nuclear Security Administration under contract DE-NA0003525.

water as well as the liberation of volatile compounds and compared the results with available experimental studies. Water is a common byproduct from both pyrolysis as well as the curing process of phenolic polymers, and the formation kinetics of water during phenolic pyrolysis have been studied in the past [9, 10]. Experimental activation energies are typically extracted via the manipulation of the mass loss curve acquired from thermogravimetry. The rationale for the second process lies in the fact that the experimental mass loss occurs due to the liberation of volatile compounds.

We studied phenol in order to probe the ability of each ReaxFF parametrization to model the intermolecular interactions inherent in phenolic polymers. Phenol is an appropriate model system that exhibits many of the same intermolecular interactions that exist in phenolic polymers due to the fact that it is the building block of phenolic polymers. We chose crystalline phenol to test the ability of each parametrization to accurately model hydrogen bonding interactions. Crystalline phenol forms a 3-fold, H-bonded helix (Fig. 1) along the crystallographic b-axis [17]. The stability of this structure at the experimental temperature serves as an indicator of the level of accuracy of the hydrogen bonding interactions of a given potential. Therefore, we studied the stability of crystalline phenol at 123 K, the temperature at which the X-ray data were collected. We also studied phenol at higher temperatures in order to determine which parametrization could most accurately model phenolics under compression at high temperatures.

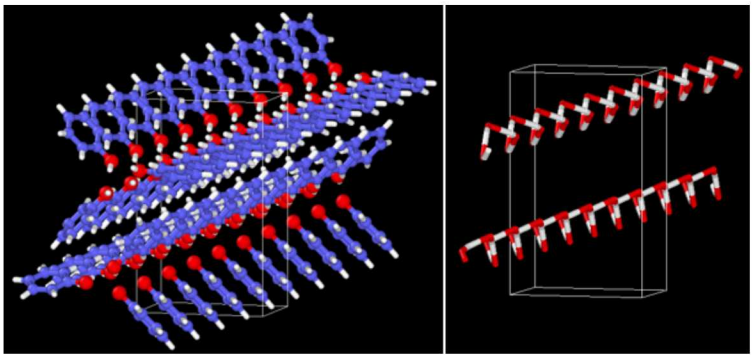

FIGURE 1. OVITO [18] visualization of the experimental x-ray crystal structure of phenol from [19]. The unit cell is replicated along the crystallographic b-axis to highlight the 3-folded helix. The image on the left contains all of the atoms. The image on the right only contains the hydrogen bonding atoms. The level of diffusion of this system during the equilibration is a metric for the ability of a ReaxFF parametrization to accurately model hydrogen bonding interactions relevant for shock.

METHODOLOGY

We carried out phenolic pyrolysis with all three ReaxFF parametrizations using constant temperature, constant volume MD at temperatures between 2000 K and 3250 K using the LAMMPS [20] MD package. Periodic boundary conditions and a 0.25 fs timestep were employed. We modelled phenolic polymer as a system of 16 linear chains, each containing 8 monomeric subunits. Phenolic polymers have been studied with MD in the past, under both reactive [9–13] and non-reactive [3, 21–23] conditions. This particular system was chosen because linear, finite mass oligomeric systems of length 8-9 have been shown to reproduce experimental pyrolysis activation energies [9, 10], shock response in the non-chemically reactive regime [5], and various thermomechanical properties [3]. We equilibrated 15 unique instances of this small, 1776 atom system, and repeated the procedure with each, averaging over them to improve the statistics. The simulations ran from tens to hundreds of picoseconds, depending on the temperature.

The kinetics of two processes were studied: the formation of water, and the liberation of volatile compounds. Volatile compounds were defined by a mass cutoff based on the heaviest compounds observed experimentally [24, 25], a number slightly greater than the mass of cresol (methylphenol). We also verified that using a slightly higher or lower mass cutoff did not significantly affect the activation energies. The activation energies associated with the liberation of volatile compounds will be referred to as "global activation energies" in this work.

The hybrid formulation was implemented with two values for p_{ovun3}, taken from the Mattsson and Chenoweth parametrizations, respectively. It was determined that the Chenoweth parameter value was better able to represent the stability of transient states, when compared to DFT. The parameter had little or no effect on activation energies.

Crystalline phenol was equilibrated with each ReaxFF parametrization for 125-350 ps at 123 K and ambient pressure, beginning with the experimental x-ray crystal coordinates from [19], and the resulting density evaluated. The

degree of crystallinity was determined by evaluating the mean squared displacement and diffusion coefficient of the system, as well as by qualitative observation of the time evolution of the 3-fold, hydrogen-bonded helix. The experimentally determined unit cell contains six molecules. This was replicated 5-fold in each direction, for a final system of 9750 atoms. Constant temperature and pressure simulations were conducted with periodic boundary conditions and a 0.1 fs timestep. A 0.25 fs timestep would likely have sufficed to accurately represent the dynamics.

For the higher temperature simulations, phenol was equilibrated at 5 different temperatures between 300 and 425 K for which experimental data are available using the same equilibration procedure that was used for the crystalline phenol. In addition to the experimental data, a NIST model was used for comparison. Specifically, the NIST ThermoData Engine [26, 27] was accessed via the NIST Web Thermo Tables application [28], which extrapolates and interpolates a wide range of available experimental data, using the EOS code REFPROP [29]. The density-temperature curve along the liquid vapor coexistence was extracted from the NIST model data, and compared with the MD results up to the critical temperature (694 K). Pressures ranged from ambient to 55 atm along the liquid/vapor coexistence.

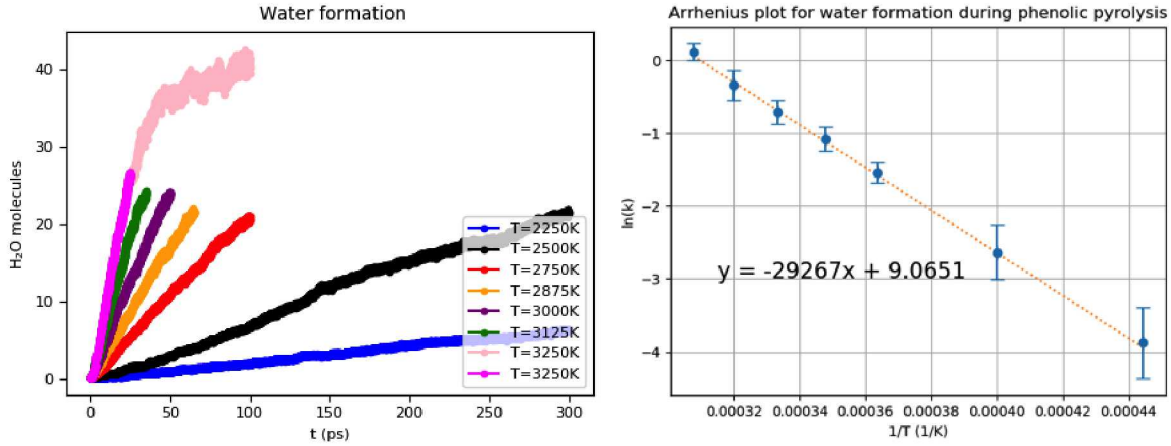

FIGURE 2. Arrhenius analysis data. Left panel: water evolution curves from MD simulations used to extract rate constants. Right panel: an Arrhenius plot.

RESULTS

Formation rates of water and of volatile compounds were extracted as a function of time for each simulation, enabling the extraction of rate constants and activation energies. These energies were averaged over 15 unique instances of the amorphous 16-chain system with a density of 1.25 g/cc (a typical density of a phenolic polymer), and compared with experimental results.

The order of both processes in the concentration of the reactant was not determined, because this dependence is insignificant, as we carried out all analyses in the limit of constant reactant concentration, where the rate of product formation is approximately constant as can be seen in the left panel of Fig. 2. The extended data for 3250 K is shown in Fig. 2 to demonstrate the breakdown of that assumption after the product is significantly consumed. The rate equation below is expressed as a first order decomposition:

$$\frac{d[\mathrm{H_2O}]}{dt} = A[\mathrm{Phenolic}] \cdot \exp\left(-\frac{E_a}{RT}\right) \tag{1}$$

$$\ln k = \ln B - \frac{E_a}{RT} \tag{2}$$

Eq. (1) can be represented as Eq. (2), where $[\mathrm{H_2O}]$ is the concentration of water and k is an effective rate constant, equal to the rate during the initial stage of pyrolysis where the concentration of phenolic, [Phenolic] is approximately constant. The initial rates of the two processes of interest, i.e. water formation and the appearance of volatile compounds, were determined for each constant temperature pyrolysis simulation and used to build the Arrhenius plot (right panel, Fig. 2) from which activation energies could be extracted. We chose the more standard natural logarithm of the rate constant for the Arrhenius plot, and recalculated the values cited from previous work

[9, 10] in Table I. Activation energies were evaluated for each of the 15 instances of the system. The average values are reported here with the error bars reported as the standard deviation. We tested other means of determining the activation energy, all yielding the same results within uncertainties.

As can be seen in Table I, the Chenoweth activation energies were consistently higher than with both the hybrid and the Mattsson parametrizations. However, all MD parametrizations yielded activation energies for water formation as well as global activation energies in agreement with experimental results, which vary widely. The wide range of the experimental data could be due to several factors. Experimentally, the activation energies of phenolic pyrolysis have been shown to vary with heating rate [30] as well as the temperature regime [31, 32] in which the analysis is carried out. Furthermore, the curing conditions for the phenolics in each study were likely not identical. Additional work is needed to compare reaction energies and activation barriers for specific, common product formation pathways using the various parametrizations with electronic structure calculations.

TABLE I. Phenolic pyrolysis activation energies.

Reference	E_a (H_2O) (kj/mol)	E_a (Global) (kj/mol)
Exp [32]	—	223-305
Exp [31]	—	74-198
Exp [30]	—	192-293
MD [9]	332(64)	—
MD [10]	286(46)	—
Chenoweth (this work)	246(23)	301(32)
Hybrid (this work)	135(5)	210(12)
Mattsson (this work)	130(6)	191(13)

We studied phenol at 123 K to determine which ReaxFF parametrization most accurately models intermolecular interactions in phenolic polymers. After equilibrating crystalline phenol using the Mattsson and Chenoweth parametrizations, it was observed that the Mattsson parametrization retains the experimental density of 1.19 g/cc to within 0.01 g/cc, but does not retain the crystal structure. The system amorphized significantly, and exhibits liquid-like behavior as indicated by the diffusion coefficient of 4.1×10^{-4} Å^2/ps, based on the slope of the fit line in Fig. 3. The left panel of Fig. 3 illustrates how far the three-fold helix has deviated from the x-ray crystal structure.

The Chenoweth parametrization retains the crystallinity as shown in Fig 3, and exhibits solid-like behavior as demonstrated in the mean squared displacement. However, the system densified by more than 20 percent of the experimental value to 1.43 g/cc.

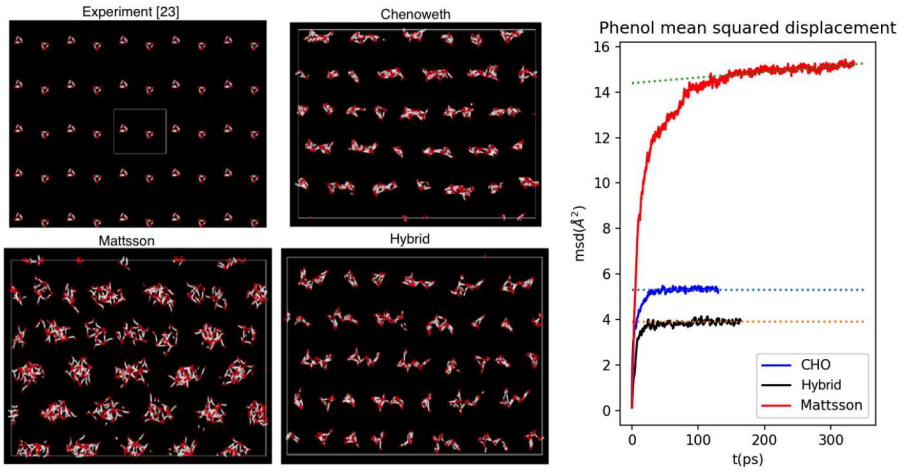

FIGURE 3. Left panel: visualization of the three fold hydrogen-bonded helix of crystalline phenol near the end of the equilibration with the three ReaxFF parametrizations. The viewpoint is oriented parallel to the crystallographic b-axis. The image in the upper left was produced using the experimental x-ray crystallography coordinates [19]. Right panel: mean squared displacement of atoms in phenol during equilibration at 123 K and ambient pressure.

In order to retain the crystallinity and the density of the system simultaneously, the hydrogen bonding parameters from the Mattsson parametrization were replaced with those of the Chenoweth parametrization. The new hybrid parametrization capitalizes on the ability of the Mattsson parametrization to maintain reasonable densities and on the ability of the Chenoweth parametrization to accurately represent hydrogen bonding interactions. Figure 3 demonstrates that the hybrid parametrization maintains the crystal structure. This new parametrization also maintains the experimental density.

Figure 4 demonstrates that our hybrid parametrization accurately models the macroscopic observables that are important for studying phenolic polymers under compression in this regime, and may be promising for future shock studies. The hybrid parametrization most accurately models phenol across a range of temperatures, in agreement with experimental data [33–35] as well as the NIST model of the liquid/vapor coexistence curve, which spans a greater temperature range, up to the critical temperature. Depending on the equilibration strategy, the hybrid parametrization can model phenol in either the liquid or vapor phase when the system is equilibrated to a temperature and pressure on the coexistence curve. Further work would be needed to fully probe the ability of the hybrid to reproduce vapor-liquid equilibrium, such as a Gibbs ensemble or large two-phase simulations.

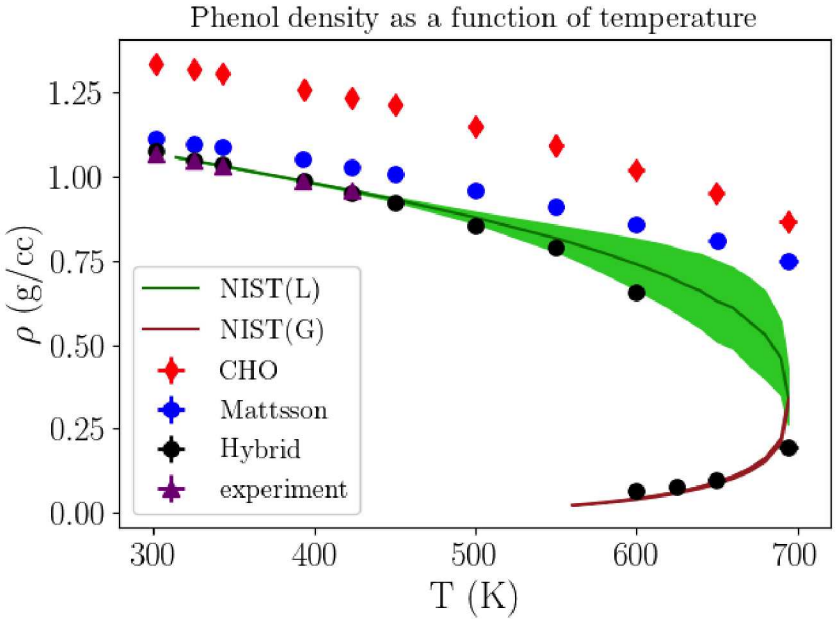

FIGURE 4. Phenol density as a function of temperature. The green and brown curves represent the NIST model for the liquid (green, uncertainty region shaded) and vapor (brown) coexistence. (Color available online).

CONCLUSIONS

We used classical MD and the ReaxFF potential to model phenolic polymers. Three parametrizations were compared in their ability to model the chemical reactions that occur during pyrolysis and to model mechanical compression due to shock. All three ReaxFF parametrizations are comparable for pyrolysis and chemistry, based on a comparison with the available experimental activation energies determined by TGA. However, our new hybrid parametrization is the most ideal ReaxFF parametrization for studying shock, due to its ability to also accurately model hydrogen bonding interactions and proper densities of a model system relevant to phenolic polymers across a range of temperatures.

ACKNOWLEDGMENTS

Sandia National Laboratories is a multi-mission laboratory managed and operated by National Technology and Engineering Solutions of Sandia, LLC., a wholly owned subsidiary of Honeywell International, Inc., for the U.S. Department of Energy's National Nuclear Security Administration under contract DE-NA0003525.

REFERENCES

1. J. Bouajila, G. Raffin, H. Waton, C. Sanglar, J. O. Paisse, and M. F. Grenier-Loustalot, Polymers and Polymer Composites **11**, 233–262 (2003).
2. N. Gabilondo, M. Larranaga, C. Pena, M. A. Corcuera, J. M. Echeverria, and I. Mondragon, J. Appl. Polym. Sci. **102**, 2623–2631 (2006).
3. J. D. Monk, E. W. Bucholz, T. Boghozian, S. Deshpande, J. Schieber, C. W. Bauschlicher, Jr., and J. W. Lawson, Macromolecules **48**, 7670–7680 (2015).
4. W. J. Carter and S. P. Marsh, *Hugoniot equation of state of polymers* (University of California Press, Berkeley, 1995).
5. B. Arman, Q. An, S. N. Luo, T. G. Desai, D. L. Tonks, T. Cagin, and W. A. G. III, J. Appl. Phys. **109**, p. 013503 (2011).
6. A. C. T. van Duin, S. Dasgupta, F. Lorant, and W. A. Goddard, III, J. Phys. Chem. A **105**, 9396–9409 (2001).
7. K. Chenoweth, A. C. T. van Duin, and W. A. Goddard, III, J. Phys. Chem. A **112**, 1040–1053 (2008).
8. T. R. Mattsson, J. M. D. Lane, K. R. Cochrane, M. P. Desjarlais, A. P. Thompson, F. Pierce, and G. S. Grest, Phys. Rev. B **81**, p. 054103 (2010).
9. D. Jiang, A. C. T. van Duin, W. A. Goddard, III, and S. Dai, J. Phys. Chem. A **113**, 6891–6894 (2009).
10. T. G. Desai, J. W. Lawson, and P. Keblinski, Polymer **52**, 577–585 (2011).
11. Y. Zhong, X. Jing, S. Wang, and Q.-X. Jia, Polym. Deg. and Stability **125**, 97–104 (2016).
12. T. Qi, C. W. Bauschlicher, Jr., J. W. Lawson, T. G. Desai, and E. J. Reed, J. Phys. Chem. A. **117**, 11115–11125 (2013).
13. A. Harpale, S. sawant, R. Kumar, D. Levin, and H. B. Chew, Carbon **130**, 315–324 (2018).
14. C. W. Bauschlicher, Jr., T. Qi., E. J. Reed, A. Lenfant, J. W. Lawson, and T. G. Desai, J. Phys. Chem. A. **117**, 11126–11135 (2013).
15. J. M. D. Lane and N. W. Moore, J. Phys. Chem. A **122**, 3962–3970 (2018).
16. J. M. D. Lane, G. S. Grest, and T. R. Mattsson, Computational Materials Science **79**, 873–876 (2013).
17. D. R. Allan, S. J. Clark, A. Dawson, P. A. McGregor, and S. Parsons, Acta. Cryst. **B58**, 1018–1024 (2002).
18. A. Stukowski, Modelling Simul. Mater. Sci. Eng. **18**, p. 015012 (2010).
19. V. E. Zavodnik, V. K. Bel'skii, and P. M. Zorkii, Zh. Strukt. Khim. **28**, p. 175 (1987).
20. S. J. Plimpton, J. Comp. Phys. **117**, 1–19 (1995).
21. J. D. Monk, J. B. Haskins, C. W. Bauschlicher, Jr., and J. W. Lawson, Polymer **62**, 39–49 (2015).
22. A. R. Pawloski, J. A. Torres, P. F. Nealey, and J. J. de Pablo, J. Vac. Sci. Technol. B **17**, 3371–3378 (1999).
23. Y. Shudo, A. Izumi, K. Hagita, T. Yamada, K. Shibata, and M. Shibayama, Macromolecules **51**, 6334–6343 (2018).
24. K. A. Trick and T. E. Saliba, Carbon **33**, 1509–1515 (1995).
25. K. A. Lincoln, AIAA Journal **21**, 1204–1207 (1983).
26. M. Frenkel, R. D. Chirico, V. Diky, X. Yan, Q. Dong, and C. D. Muzny, J. Chem. Inf. Model. **45**, 816–838 (2005).
27. V. Diky, C. D. Muzny, E. W. Lemmon, R. D. Chirico, and M. Frenkel, J. Chem. Inf. Model. **47**, 1713–1725 (2007).
28. K. G. Kroenlein, C. D. Muzny, V. Diky, R. D. Chirico, J. W. Magee, I. M. Abdulagatov, and M. D. Frenkel, Nist/trc web thermo tables (wtt) nist standard reference subscription database, 2011.
29. E. W. Lemmon, I. Bell, M. L. Huber, and M. O. McLinden, NIST Standard Reference Database 23: Reference Fluid Thermodynamic and Transport Properties-REFPROP, Version 10.0, National Institute of Standards and Technology, 2018.
30. H. L. Freidman, J. Polym. Sci. C **6**, 183–195 (1964).
31. K. A. Trick, T. E. Saliba, and S. S. Sandhu, Carbon **35**, 393–401 (1997).
32. H. Jiang, J. Wang, S. Wu, B. Wang, and Z. Wang, Carbon **48**, 352–358 (2010).
33. R. B. B. and, J. Chem. Eng. Data **10**, p. 143 (1965).
34. D. L. Cunha, J. A. P. Coutinho, J. L. Daridon, R. A. Reis, and M. L. L. Paredes, J. Chem. Eng. Data **58**, 2925–2931 (2013).
35. C. A. Buehler, J. H. Wood, D. C. Hull, and E. C. Erwin, J. Am. Chem. Soc. **54**, 2398–2405 (1932).